# Proposed new failure criterion for bending stiffeners

*Author Names: Luciano Valdomiro dos Santos / Edison Gonçalves*
Petropasy Polyurethane Technology
Department of Mechatronics Engineering and Mechanical Systems (Polytechnic School, University of São Paulo)
São Paulo, São Paulo, Brazil

## ABSTRACT

This paper presents a new failure criterion for bending stiffeners for flexible pipes, a metal-polymer structure used by the oil and gas industry, which takes into consideration the failure in the metal-polymer interface region due to sliding wear, when there is relative movement between the surfaces. Initially, presents bending stiffeners. It then shows the stiffener bending characteristics. Soon after, presents the proposed failure criterion and, finally, shows a sliding test performed to validate the proposed failure criterion.

KEY WORDS: bending stiffener; flexible pipe; sliding wear.

## INTRODUCTION

The bending stiffeners are structures composed of a polymeric part, usually made from thermoplastic polyether polyurethane [LEMOS 2005] anchored to a metallic part which is intended to allow the installation of the assembly in the place of use. They are responsible for the smooth transition of stiffness between a very flexible structure flexible line (riser or umbilical), and one which is extremely rigid that is structure of an oil platform (figure 1).

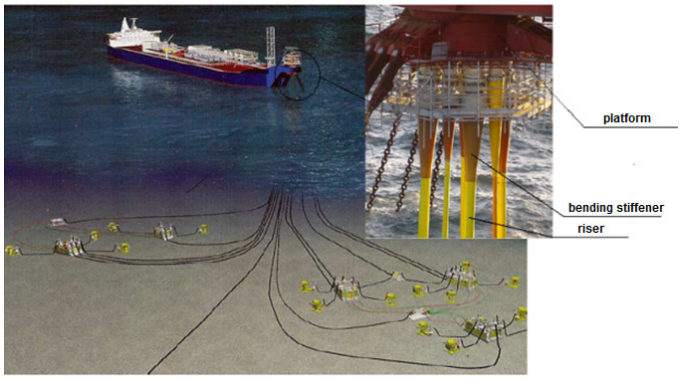


Figure 1 – Bending stiffener, FPSO platform and risers, [CAIRE, 2005].

The flexible lines have been increasingly used in applications for offshore oil exploration in recent years. They are used to transport various types of fluids, usually at high pressure. They have several metal layers combined with concentric polymeric layers to form a structure with high torsional and axial rigidity, but a low flexural rigidity, [LEMOS, 2005].

The bending stiffeners appeared due the need to avoid very small radii of curvature that can damage the structure of the flexible lines used in offshore oil exploration. The correct evaluation of bending stiffeners can mean the difference between safe operation of a flexible line or from your failure, especially in the case of units of FPSO platforms (Floating Production, Storage and Offloading) or more critically in single point mooring [LEMOS, 2005]. The monobuoys, especially in deep water, can lead to extreme situations flexible lines that besides suffering from high tensile loads, they are subject to high bending stresses imposed by monobuoy movements. This has aroused great concern in the oil companies, in particular, at Petrobras, especially after the failures recorded in the Campos Basin in 1998 and 1999, when the stiffeners to bending of monobuoy IMODCO III in the Marlim field, after six months of operation, suffered failure [POPE, 1998]. A lot of stiffeners of the same project continue in operation in some FPSOs causing concern over its useful life, [CAIRE, 2005]. The failure analysis of bending stiffeners led to the conclusion that the predominant failure mechanism was initiated by the polymer fatigue, [POPE, 1998].

## BENDING STIFFENER

The bending stiffeners are composed of a polymeric part anchored to a metallic insert (see Figure 2).

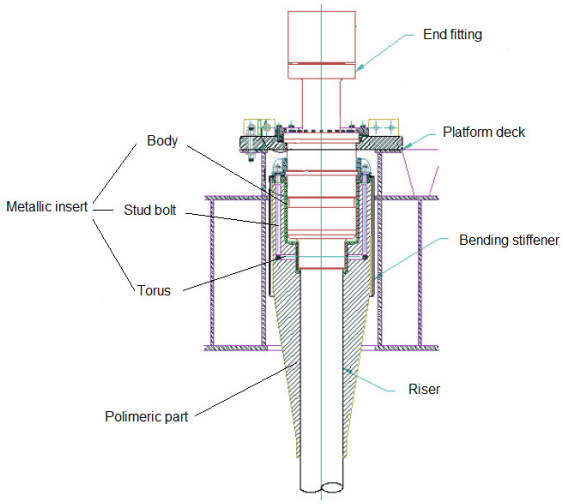


Figure 2 – Bending Stiffener, [CLEVELARIO].

The metallic insert is essentially composed of a stepped welded metal body and a toroidal ring welded to stud bolts, which are perpendicularly arranged axially in relation to said toroidal ring and the flange of the metal body (see figure 3). This configuration forms a kind of cage that surrounds the circumference of the flexible line. Thus when the polymeric part of the bending stiffener is subjected to external bending, the insert keeps anchored the base of the bending stiffener. The cage configuration is ideal for ensuring the anchoring of the polymeric part. The main problems of metallic insert are:

- Impossibility to sizing to infinite life, even under ideal conditions;
- Necessity of execution of various nondestructive testing for the verification of welded joints;
- Presence of discontinuities in welds inherent to the process;
- Difficulty to ensure the roughness of the interface areas with the polymeric part by the fact that it is obtained by manual grinding and polishing.

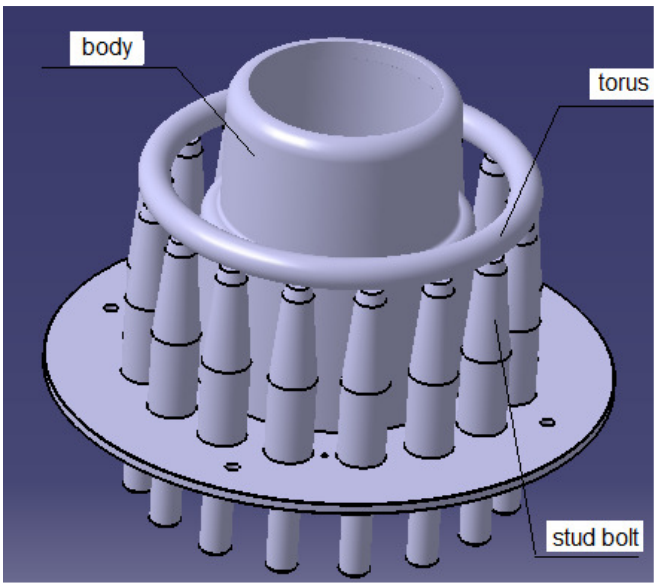

Figure 3 – Metallic insert, [SANTOS, 2014].

Due to these problems, the use of expensive super alloy (inconel 625, for example) is required for the construction of the metallic insert.

Table 1 shows the relevant properties of each material used in the construction of bending stiffeners. Note that if the cost of Inconel 625 is twenty-five times greater than that of structural steel SAC 350 USI.

The manufacture of the bending stiffener is a complex process. Essentially the operation entails the construction of a mold tool. A center tube is positioned within an outer shell forming a cavity the shape of the required component. The metallic insert is placed in the base unit bottom sealing tool as shown in Figure 4. The metallic body of the insert is coated with a suitable adhesive. The toroidal ring and the stud bolts of the metallic insert, together with the inner surfaces of the tool are treated with a release agent prior to assembly. Prior to filling the mold is heated to a suitable temperature. The polyurethane is then fed through a filling hole usually located at the bottom of the mold. The liquid rises, displacing air from the cavity through a hole, which is usually located at the highest point of the assembly. When the filling operation is completed, the initial curing of the material takes place with the reaction and solidification of polyurethane. The solidified component is then demolded and subjected to detailed inspection before being approved. This manufacturing process is designed to ensure perfect adhesion between the polyurethane and the body of the insert, and a slip between the polyurethane and the torus insert.

Table 1 – Properties of materials used in bending stiffener, [SANTOS, 2014].

| **Bendig Stiffener parts** | | **Insert body** | **Insert stud bolt and torus** | **Polimeric part** |
|---|---|---|---|---|
| **Property** | | **USI SAC 350** | **Inconel 625 annealed** | **Thermoplastic polyurethane polyether** |
| **Carbon [%]** | | Máx. 0,25 | Máx. 0,10 | |
| **Manganese [%]** | | Máx. 1,5 | Máx. 0,50 | |
| **Sulfur [%]** | | Máx. 0,02 | Máx. 0,015 | |
| **Phosphorus [%]** | | 0,01 a 0,06 | Máx. 0,015 | |
| **Silicon [%]** | | 0,5 a 1,50 | Máx. 0,50 | |
| **Chrome [%]** | | Máx. 0,60 | 20 a 23 | |
| **Molybdenum [%]** | | | 8 a 10 | |
| **Nickel [%]** | | | Mín. 58 | |
| **Iron [%]** | | | Máx. 5,0 | |
| **Niobium [%]** | | | 3,15 a 4,15 | |
| **Copper [%]** | | 0,05 a 0,4 | | |
| **Modulus of elasticity [GPa]** | | 190 a 210 | 208 | 0,045 |
| **Poisson's Ratio** | | 0,27 a 0,30 | 0,28 | |
| **Tensile strength [MPa]** | | 500 a 650 | 827 a 1034 | 42 |
| **Yield strength [MPa]** | | Mín. 350 | 415 a 655 | |
| **Elongation [%]** | | Mín. 16 | 30 a 60 | 325 |
| **Average Impact Resistance [J]** | | | 66 (29ºC) / 57 (-79ºC) | |
| **Fatigue strength [MPa]** | **$10^4$ cycles** | | | |
| | **$4x10^4$ cycles** | | | |
| | **$10^5$ cycles** | | | |
| | **$4x10^5$ cycles** | | | |
| | **$10^6$ cycles** | | 655 | |
| | **$4x10^6$ cycles** | | | |
| | **$10^7$ cycles** | | 630 | |
| | **$10^8$ cycles** | | 621 | |
| **Cost [USD/kg]** | | 4,00 | 100,00 | |

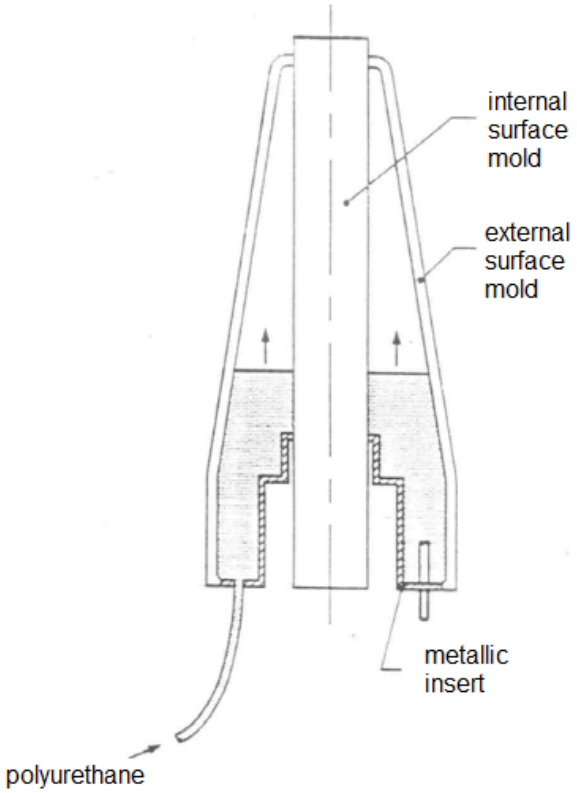

Figure 4 – Mold for bending stiffener, [KIEPPER, 2004].

The main potential defects of a bending stiffener are [API 1999]:

- Cracking of the polymeric part;
- Breaking of the polymeric part;
- Structural failure of the insert;
- Performance loss of the polymeric part.

One possible cause for the first three defects is the fatigue mechanism [API 1999]. The main points of failure due to fatigue are shown in figure 5, [DEMANZE, 2005].

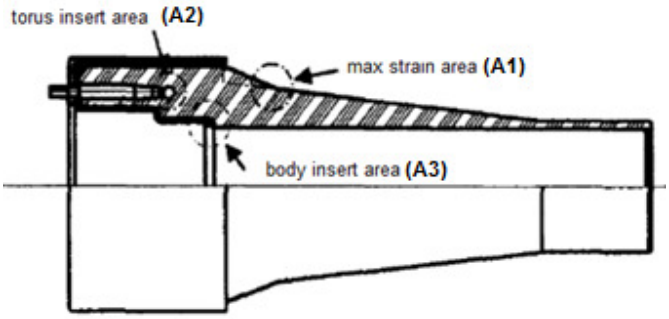


Figure 5 – Critical areas to fatigue failure, [DEMANZE, 2005].

It is noticed that two critical regions are located at the interface of the polymeric part with the metallic part of the bending stiffener, that is, the anchorage area, where cracks are most likely nucleated due to failure by sliding, which is strongly influenced by surface roughness, [HUTCHINGS, 1992].

## FAILURE CRITERION PROPOSED

Assuming the hypothesis that the wear rate is related to the number of deformation cycles required to remove an asperity through of the fatigue process, [HUTCHINGS, 1992], suggesting the possibility of using a S-N curve for obtaining the number of cycles required to release a wear particle. Another hypothesis adopted for the use of this concept is that the topography of a surface with small dimensions presents similar boundary of topography of a surface with large dimensions thus enabling the application of theories studying macro scales phenomena to explain micrometers phenomena. It is considered a flexible body with $e$ thickness in contact with a rigid body (Figure 6) where topographies fit perfectly in motion by applying a tangential force $P_t$. The permanent pressure exerted by the normal force P is considered to be the apparent pressure, i.e., the ratio of the force by area:

$$\text{apparent pressure} = \frac{P}{A} = \frac{P}{L\,e} \tag{1}$$

The sum of the forces $P_a$ exercised on the ramp of each asperity due to tangential force $P_t$ is:

$$\sum P_a = P_t \sin\theta \tag{2}$$

The sum of the areas of the ramps of each asperity $A_a$ is:

$$\sum A_a = \frac{\sum h\,e}{\sin\theta} \tag{3}$$

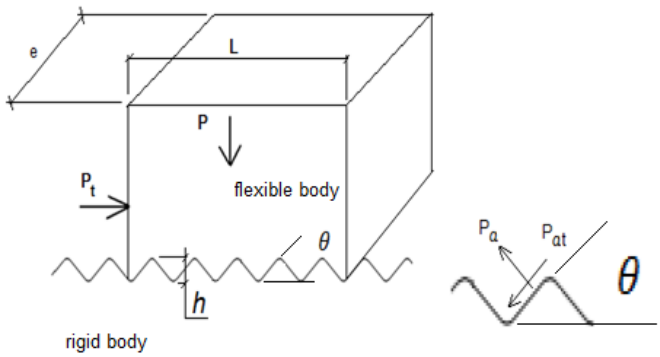


Figure 6 – Contact between flexible body and rigid body.

Therefore, the pressure in the ramp of each asperity due to the motion:

$$\sigma = \frac{\sum P_a}{\sum A_a} \tag{4}$$

$$\sigma = \frac{P_t \sin\theta}{\sum h\,e\,/\sin\theta} \tag{5}$$

$$\sigma \frac{P_t}{\sum h\,e} \sin^2\theta \tag{6}$$

Since:

$$P_t = \mu\,P \tag{7}$$

Where μ is the friction coefficient:

$$\sigma = \frac{\mu\,P}{\sum h\,e} \sin^2\theta \tag{8}$$

Once the pressure in each ramp asperity is:

- Initial instant = apparent pressure;
- Passage of an asperity by the other = apparent pressure + σ;
- After passage of an asperity by the other = apparent pressure.

In this case, the equivalent alternating stress amplitude calculation is required since the average stress is different than zero.

The sum of $P_{at}$ forces exerted on the ramp of each asperity due to $P_t$ tangential force is:

$$\sum P_{at} = P_t \cos\theta \tag{9}$$

The sum of the areas of the ramps of each asperity $A_a$ is:

$$\sum A_a = \frac{\sum h\,e}{\sin\theta} \tag{10}$$

Therefore, the shear stress exerted on each ramp asperity due to movement in case there was a complete junction asperities (welding), it would be:

$$\tau_1 = \frac{\sum P_{at}}{\sum A_a} \tag{11}$$

$$\tau_1 = \frac{P_t \cos\theta}{\sum h\, e / \sin\theta} \quad (12)$$

$$\tau_1 = \frac{P_t}{\sum h\, e} \cos\theta \sin\theta \quad (13)$$

Again using equation 7, results in:

$$\tau_1 = \frac{\mu P}{\sum h\, e} \cos\theta \sin\theta \quad (14)$$

As there is no complete junction of asperities, only a portion of the tangential force $P_{at}$ due the adhesion friction coefficient generates shear stress, we have:

$$\tau_1 = \frac{\mu P \mu_{adesão}}{\sum h\, e} \cos\theta \sin\theta \quad (15)$$

Once the shear stress in each ramp asperity is:

- Initial instant = 0;
- Passage of an asperity by the other = $\tau_1$;
- After passage of an asperity by the other = 0.

In this case, it is also necessary to calculate the equivalent alternating stress amplitude since the average stress is different than zero.

It is noted the application of an alternating compressive pressure and an alternating shear stress in the asperity ramp. The compressive stresses do not cause fatigue failure. However, as shown by Hertz analysis, applying a normal pressure produces a shear stress below the surface. This shear stress is equal to 0.47 times the normal pressure, and the cyclic variation that may cause fatigue failure of the asperity. Therefore, from equation 8 we have:

$$\tau_2 = 0.47 \frac{\mu P}{\sum h\, e} \sin^2\theta \quad (16)$$

The schematic model for detachment of the asperity showed in the figure 7 is proposed, valid only when the contact is fully elastic, where most of life (cycles) is spent for crack nucleation.

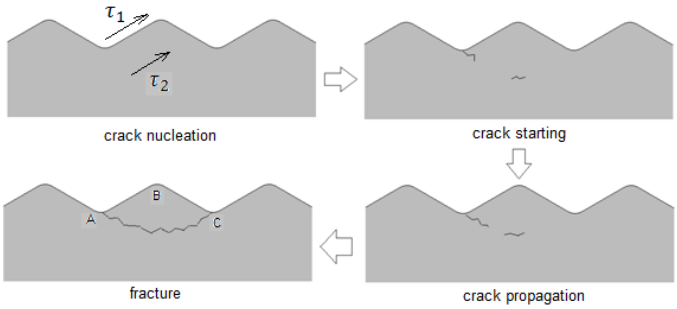


Figure 7 – Schematic model for asperity failure due fatigue.

Thus, the wear rate can be estimated considering the following variables: height of asperity, the asperity angle, normal force, number of cycles (depending on the slide length), the coefficient of friction and the curve of fatigue resistance of the material. The volume of each removed asperity is considered to be the product of two times the area of triangle ABC shown in Figure 7 by the thickness of the flexible body. The fatigue strength curve should consider the fatigue strength modification factors. A practical way to discovery of a proposed overall reduction ratio (CGR) resistance to fatigue of the material is by adjusting for wear rate calculated for a certain asperity angle to values close to a wear rate obtained experimentally for the same asperity angles. This overall reduction coefficient also makes the implementation of the calculation of the equivalent alternating stress amplitude is not necessary, since the resistance to material fatigue curve is set to a condition where the average voltage is different than zero. For direct use of the S-N curve, the following equation is proposed:

$$\sigma_a = CGR \frac{\tau_1 + \tau_2}{2} \quad (17)$$

To validate the proposed model, this was applied to the prediction of known wear rates of 6.6 nylon and polystyrene shown in Figure 8. The following parameters were adopted for the two materials:

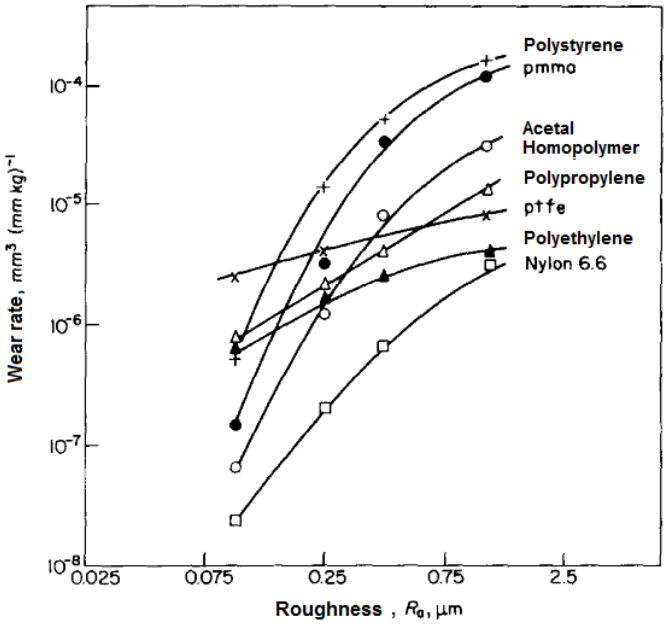


Figure 8 – Wear rate in function on roughness for several polymers in abrasion of single pass, [LANCASTER, 1972].

- P = 100 N
- L = 12 mm
- E = 12 mm
- h = 0,8 µm
- θ = 1,7° / 4° / 7° / 11°
- Sliding length = 500 m
- µ = 0,4
- $\mu_{adhesion}$ = 0,1

The S-N curves of these two polymers are shown respectively in Figures 9 and 10. I was used a CGR 562 for nylon and 220 for polystyrene. This factor was obtained by adjusting the rate of wear obtained for the angle 4° with that found in Figure 8. Table 2 shows the calculated wear rates.

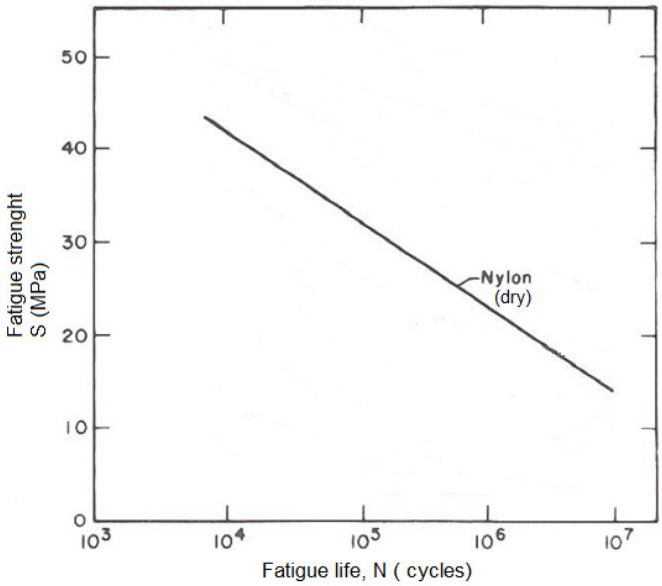


Figure 9 - S-N curve nylon, [HERTZBERG, 1980].

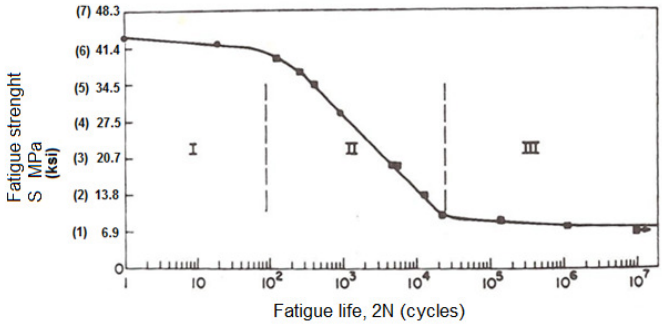


Figure 10 - S-N curve polystyrene, [HERTZBERG, 1980].

Table 2 – Calculated wear rates using the proposed model.

| Asperity angle [degree] | $\tau_1$ [MPa] | $\tau_2$ [MPa] | CGR | $\sigma_a$ [MPa] | Fatigue life [N] | Wear rate [mm3/(Nm)] | Material |
|---|---|---|---|---|---|---|---|
| 1,7 | 0,06 | 0,008 | 562 | 17,8 | 4,00E+06 | 5,3E-06 | NYLON THEORY |
| 4 | 0,06 | 0,018 | 562 | 20,6 | 2,00E+06 | 2,5E-05 | |
| 7 | 0,05 | 0,032 | 562 | 24,3 | 8,00E+05 | 1,1E-04 | |
| 11 | 0,05 | 0,049 | 562 | 28,8 | 2,00E+05 | 7,0E-04 | |
| 1,7 | 0,06 | 0,008 | 220 | 7,0 | 5,00E+05 | 4,3E-05 | PS THEORY |
| 4 | 0,06 | 0,018 | 220 | 8,1 | 5,00E+04 | 1,0E-03 | |
| 7 | 0,05 | 0,032 | 220 | 9,5 | 1,00E+04 | 8,8E-03 | |
| 11 | 0,05 | 0,049 | 220 | 11,3 | 5,00E+03 | 2,8E-02 | |

The values obtained were plotted for comparison, in the diagrams of figure 8. The wear rates figure 11 shows the comparison.

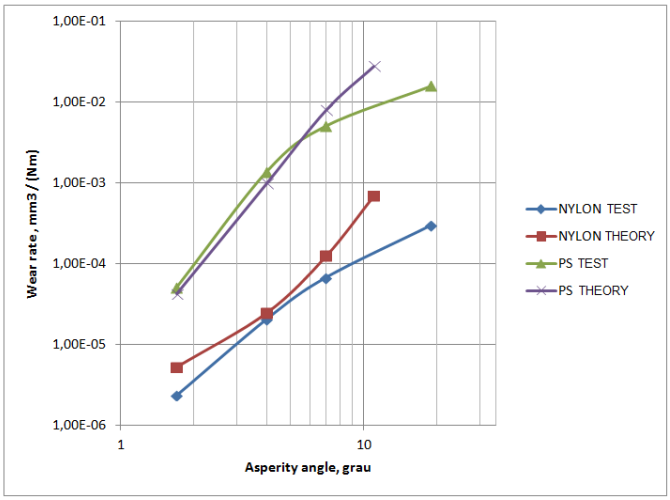


Figure 11 – Comparative wear rates obtained in tests and calculated.

It shows a good correlation of the model with experimental results for asperities angles below than 10 degrees.

## SLIDING TEST

To survey the rate of wear by sliding polyurethane, which was not found in literature, sliding tests were carried out in alternating lay flat plane. Cylindrical specimens with a diameter of 12 mm and a height of 5 mm of polyurethane 95 Shore A to 55 Shore D hardness, were taken from round bars provided by Petropasy, a bending stiffener manufacturer, and encapsulated in a layer of low-carbon steel. These were brought into contact against the low-carbon steel plates with two different topographies a sanded by hand and another thick rectified, both with risks in the transverse direction. The schematic configuration of the test is shown in Figure 12.

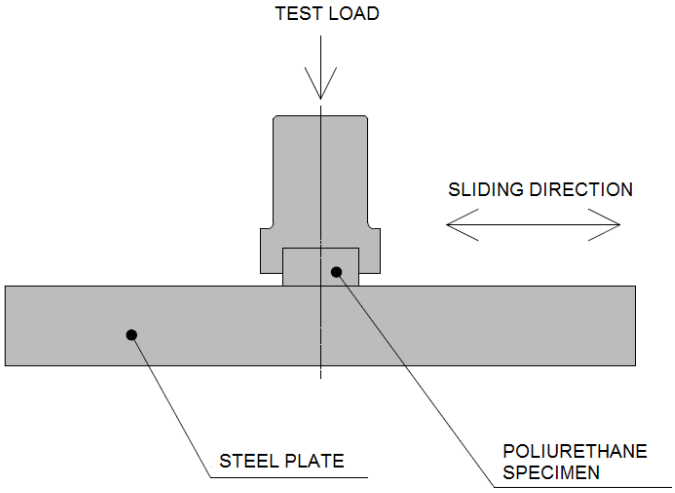


Figure 12 – Sliding test schematic configuration.

Figure 13 shows the test apparatus with 10 kgf load coupled to a test equipment.


Figure 13 – Test equipment with 10 kgf load.

Topographies of steel plates sanded and rectified thick were measured in interferometer. The sanded steel plate had an average angle of the asperity of 11.02 degrees and average roughness of 0.98 µm. The rectified thick steel plate had an average angle of the asperity of 15.96 degrees and average roughness of 1.53 µm.

The form chosen for the control of the wear of the specimens was through mass loss measurement at the end of each test. The test load was 10 kgf. This was chosen so as to maintain contact within the elastic zone. In order to avoid changing the properties of the specimens due to heating, the tests were performed at a frequency of 1.15 Hz (69 cycles per minute). The adjusted stroke in test equipment was 10 mm (20 mm total travel of the end of the cycle). The results of 13 trials are shown in Table 3. A plot of these results is shown in figure 14.

Table 3 – Results of the sliding test.

| No specimen | Hardness | Roughness [um] | Sliding lenght [m] | Weight loss [g] | Volume loss [mm3] | Wear rate [mm3 / (Nm)] |
|---|---|---|---|---|---|---|
| 1 | 95 Shore A | 1 | 201 | 0,0004 | 0,333 | 1,7E-05 |
| 2 | 95 Shore A | 1 | 119 | 0,0006 | 0,500 | 4,3E-05 |
| 3 | 95 Shore A | 1 | 212 | 0,0004 | 0,333 | 1,6E-05 |
| 4 | 95 Shore A | 1,5 | 76 | 0,0022 | 1,833 | 2,5E-04 |
| 5 | 95 Shore A | 1,5 | 50 | 0,0015 | 1,250 | 2,6E-04 |
| 6 | 95 Shore A | 1,5 | 25 | 0,0005 | 0,417 | 1,7E-04 |
| 7 | 95 Shore A | 1,5 | 33 | 0,0009 | 0,750 | 2,3E-04 |
| 8 | 55 Shore D | 1 | 200 | 0,0001 | 0,083 | 4,3E-06 |
| 9 | 55 Shore D | 1 | 262 | 0,0003 | 0,250 | 9,7E-06 |
| 10 | 55 Shore D | 1,5 | 25 | 0,0019 | 1,583 | 6,5E-04 |
| 11 | 55 Shore D | 1,5 | 41 | 0,0030 | 2,500 | 6,2E-04 |
| 12 | 55 Shore D | 1,5 | 50 | 0,0009 | 0,750 | 1,5E-04 |
| 13 | 55 Shore D | 1,5 | 30 | 0,0019 | 1,583 | 5,4E-04 |

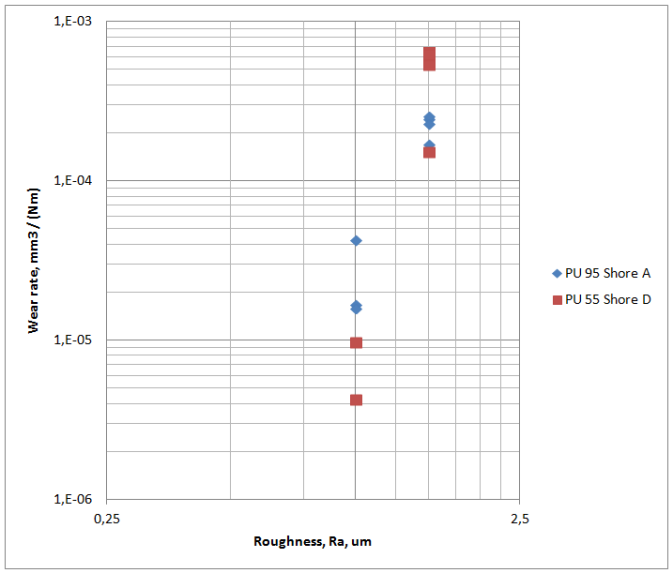


Figure 14 – PU wear rate as a function of surface roughness.

The average results for each test condition (hardness polyurethane versus surface roughness of the counter) are shown in table 4. The plot of these results is shown in figure 15.

Table 4 – Average results of sliding tests.

| Hardness | Roughness [um] | Wear rate [mm3/(Nm)] |
|---|---|---|
| 95 Shore A | 1 | 2,5E-05 |
| 95 Shore A | 1,5 | 2,3E-04 |
| 55 Shore D | 1 | 7,0E-06 |
| 55 Shore D | 1,5 | 4,9E-04 |

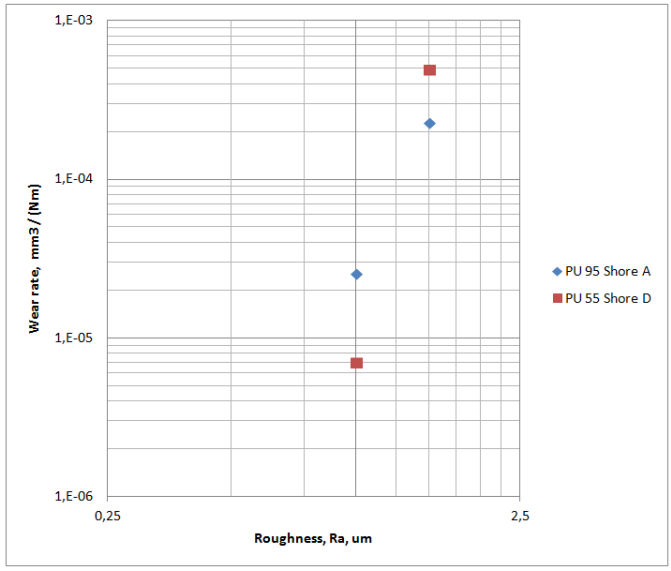


Figure 15 – PU average wear rate as a function of surface roughness.

It was noted that if increasing the hardness of the polyurethane wear rate decreases at low surface roughness and increases the wear rate in high surface roughness. Table 5 shows the wear rate calculated using the proposed model. The following parameters were adopted for the polyurethane:

- P = 100 N
- L = 12 mm
- E = 12 mm
- h = 0,8 µm
- θ = 11° / 16°
- Sliding length = 500 m
- µ = 0,4
- $\mu_{adhesion}$ = 0,1

The S-N curve of this polymer is shown Figure 16. It was used a factor of 41 for the CGR. This was achieved by adjusting the result for the angle of 11° with that found in Figure 15.

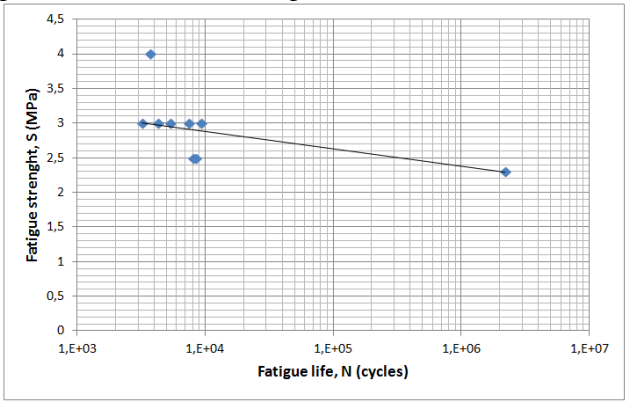


Figure 16 - S-N curve polyurethane constructed from results in the literature, [MEAD, 1985].

Table 5 – Calculated wear rates using the proposed model.

| Asperity angle [degree] | $\tau_1$ [MPa] | $\tau_1$ [MPa] | CGR | $\sigma_a$ [MPa] | Fatigue life [N] | Wear rate [mm3/(Nm)] |
|---|---|---|---|---|---|---|
| 11 | 0,05 | 0,049 | 41 | 2,1 | 1,00E+07 | 1,4E-05 |
| 16 | 0,05 | 0,069 | 41 | 2,5 | 3,00E+05 | 6,9E-04 |

The values obtained were plotted for comparison, in the diagrams of figure 8. The wear rates figure 17 shows the comparison with the inclusion of the polyurethane wear rates obtained in testing and calculated by the model proposed.

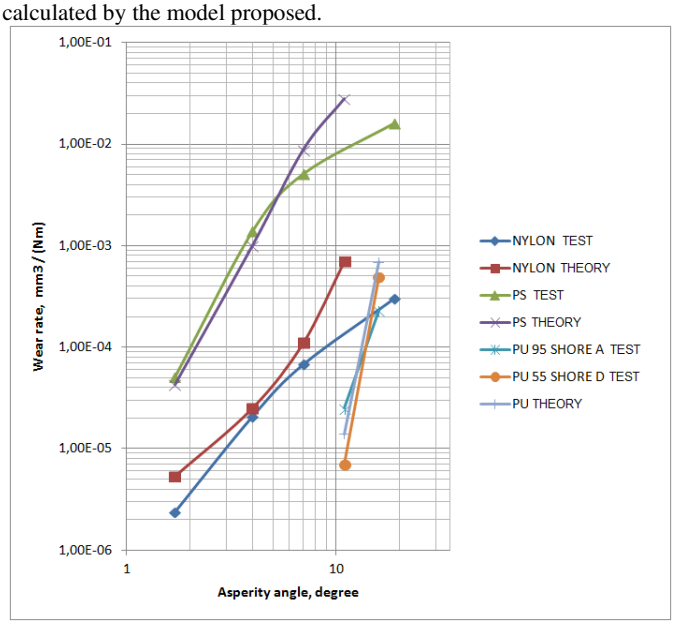


Figurer 17 – Comparative wear rates obtained in tests and calculated.

It was noted a good correlation of the model with the experimental results for the polyurethane.

Figure 18 shows the plot of wear rates for the polyurethane 95 Shore A obtained experimentally and through the proposed model for asperity angle 16 degree in a figure with Lancaster, Ratner correlation of other polymers, [LANCASTER, 1972] . The correlation Lancaster, Ratner was calculated using the average mechanical properties of the polyurethane 95 Shore A obtained in literature [MORAES, 2005]. It was noted a good convergence of values.

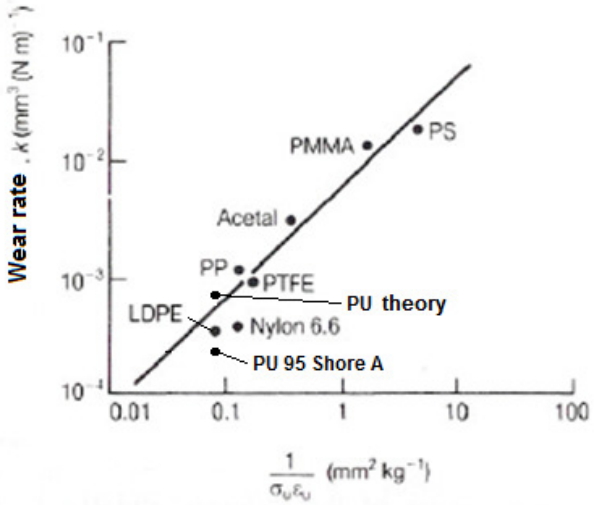


Figure 18 – Ratner-Lancaster correlation between the polymer wear rates under predominantly abrasive conditions and reciprocity of the product of stress and strain at rupture.

It was concluded that the proposed method can be used with great reliability for the evaluation of varying wear rates in function of change topography in situations where the asperity failure occurs due fatigue.

## RESULT ANALYSIS

Considering the relative movement of the polymer in relation to the metal insert torus, occurring in region A2 of the bending stiffener (Figure 5), the proposed failure criterion can be used to estimate the stress level in polymeric portion due to the roughness of the metal part. It may be noted in Table 5, that a roughness increase from 1.0 µm to 1.5 µm (asperity angle from 11° to 16°) induces a 19% increase in the alternating stress amplitude. Therefore, to predict the fatigue life in the A2 region of the bending stiffener, a fatigue strength reduction factor, due to increased surface roughness, can be considered as being around 0.84 [SANTOS, 2014].

## CONCLUSIONS

The main conclusion of this study is that the proposed analysis model, using the polymer sliding wear rate as function of the asperity angle, is reliable to predict the surface fatigue failure. The proposed model demonstrated to be valid only for high cycle fatigue failure, where the asperity crack initiation period consumes the highest percentage of fatigue life.

REFERENCES


API Recommended Practice 17B Recommend Practice For Flexible Pipe. AMERICAN PETROLEUM INSTITUTE, 1999.

CAIRE, M. Bending Stiffeners Analysis. 2005. 115 f. Dissertation (Master of Science), COPPE/UFRJ, Rio de Janeiro, RJ, Brazil, 2005.

CLEVELARIO, J. Introduction to Unbonded Flexible Pipe Design and Manufacturing. USP Course on Flexible Pipes.

DEMANZE, F. et al. Fatigue Life Analysis of Polyurethane Bending Stiffeners. Proceedings of 24th International Conference on Offshore Mechanics and Arctic Engineering. OMAE 2005-67506, Halkidiky, Greece, June 2005.

HERTZBERG, R. W.; MANSON, J. A.. Fatigue of Engineering Plastics. New York: Academic Press, Inc, 1980.

KIEPPER, B.O. Structural Static Analysis, by Finite Element of the Riser-Bending Stiffener segment. 2004. 95 f. Dissertation (Master of Science), COPPE/UFRJ, Rio de Janeiro, RJ, Brazil, 2004.

LANCASTER, J. K.. Friction and Wear. Chapter 14. Polymer Science, A Materials Science Handbook. Ed. Jenkins A. D.. North Holland Publishing Co. 1972.

LEMOS, C. A. D. Fatigue Analysis in Risers. 2005. 248 f. Thesis (Doctor of Science) - COPPE/UFRJ, Rio de Janeiro, RJ, Brazil, 2005.

MEAD, J. L.. Mechanical Degradation of a Polyurethane Elastomer. 1985. 126 f. Thesis (Doctor of Philosophy) – MIT, Massachusetts, EUA, 1985.

MORAES, J. O.et al. Effect of Mechanical Properties on Abrasive Wear Polyurethanes MDI-BD. 15º POSMEC – Symposium of the Graduate Program in Mechanical Engineering, Minas Gerais, Brazil, 2005

POPE, A. M.; CARDOSO, L. G. C.; SANTOS, J. M. Failure Analysis of Bending Stiffener of IMODCO III monobuoy. Internal technical communication Petrobras No 127/08; CENPES/SUSEP/DIPLOT/SEMEC. October 1998.

SANTOS, L.V. Failure analysis of metal-polymer structures: bending stiffeners. 2014. 129 f. Thesis (Doctorate in Mechanical Engineering) - POLI/USP, São Paulo, SP, Brazil, 2014.